https://ntrs.nasa.gov/search.jsp?R=20170001624 2018-10-22T05:53:31+00:00Z

Conceptual Feasibility Study of the Hyperloop Vehicle for Next-Generation Transport

Kenneth Decker,* Jeffrey Chin,† Andi Peng,‡ Colin Summers,§
Golda Nguyen,¶ Andrew Oberlander,‖ Gazi Sakib,** Nariman Sharifrazi,††
Christopher Heath,† Justin Gray,† Robert Falck, ‡‡

NASA Glenn Research Center, Cleveland, OH

The Hyperloop concept is proposed as a faster, cheaper alternative to high-speed rail and traditional short-haul aircraft. It consists of a passenger pod traveling through a tube under light vacuum while being propelled and levitated by a combination of permanent and electro-magnets. The concept addresses NASA's research thrusts for growth in demand, sustainability, and technology convergence for high-speed transport. Hyperloop is a radical departure from other advanced aviation concepts, however it remains an aeronautics concept that tackles the same strategic goals of low-carbon propulsion and ultra-efficient vehicles.

System feasibility was investigated by building a multidisciplinary vehicle sizing model that takes into account aerodynamic, thermodynamic, structures, electromagnetic, weight, and mission analyses. The sizing process emphasized the strong coupling between the two largest systems: the tube and the passenger pod. The model was then exercised to examine Hyperloop from a technical and cost perspective. The structural sizing analysis of the travel tube demonstrates potential for significant capital cost reductions by considering an underwater route. Examination of varying passenger capacity indicates that the system can be operated with a wide range of passenger loads without significant change in operating expenses. Lastly, a high-level sizing study simulated variations in tube area, pressure, pod speed, and passenger capacity showing that there is a tube pressure that minimizes operating energy usage. The value of this optimal tube pressure is highly sensitive to numerous design details. These combined estimates of energy consumption, passenger throughput, and mission analyses all support Hyperloop as a faster and cheaper alternative to short-haul flights.

The tools and expertise used to quantify these results also demonstrate how traditional aerospace design methods can be leveraged to handle the complex and coupled design process. Much of the technology development required for the Hyperloop is shared with next-generation aircraft. Furthermore, the substantial public interest and active commercial development make it an ideal candidate as an aircraft technology driver and test bed.

*Aerospace Engineer, Georgia Insitute of Technology, Aerospace Systems Design Lab
†Aerospace Engineer, Propulsion Systems Analysis Branch, Mail Stop 5-11, AIAA Member
‡Computer Scientist, Global Affairs, Yale University
§Chemical Engineer, Computer Engineer, University of Washington-Seattle
¶Mechanical Engineer, Georgia Institute of Technology
‖Mechanical Engineer, Brown University
**Physics, Mechanical Engineer, Stony Brook University
††Aerospace Engineer, Mechanical Engineer, University of California-Irvine
‡‡Aerospace Engineer, Mission Architecture and Analysis Branch, Mail Stop 162-2, AIAA Member

Nomenclature

α	Weighting factor
β	Magnetic Field Strength (T)
δ^*	Boundary layer thickness (m)
$\frac{u}{U}$	Boundary Velocity Profile
γ	Heat Capacity Ratio
λ	Wavelength (m)
$\mathcal{E}$	Energy (J)
ν	Kinematic Viscosity ($\frac{m^2}{s}$)
ν_{Poi}	Poisson Ratio
ω	Frequency (Hz)
Π	Pressure Ratio
ρ	Density ($\frac{kg}{m^3}$)
ε	Expansion ratio
A	Area (m^2)
A^*	Throat Area (m^2)
bm	Bond maturity (years)
C	Cost (USD)
C_D	Coefficient of drag
C_p	Heat capacity at constant pressure ($\frac{J}{kgK}$)
D	Length (m)
d	Thickness (m)
d_c	Track strip spacing (m)
E	Elastic modulus (Pa)
F	Force (N)
g	Gravitational acceleration ($\frac{m}{s^2}$)
h	Height (m)
ib	Bond interest rate
k	Thermal Conductivity ($\frac{W}{mK}$)
L	Inductance (H)
M	Mach Number
m	Mass (kg)
m'	Mass per length ($\frac{kg}{m}$)
P	Power (W)
p	Pressure (Pa)
Pr	Prandtl Number
Q	Heat energy (J)
R	Resistance (Ω)
r	Radius (m)
Re	Reynold's number
T	Temperature (K)
t	Time (variable)
u_P	Pump uptime per day
v	Velocity ($\frac{m}{s}$)
w_{mag}	Magnet Width (m)
x	Distance along tube axis (m)
y	Distance normal to flow (m)

I. Introduction

Motivation Currently, flying is the fastest and cheapest way for commercial passengers to travel long distances. However, for shorter routes the efficiency of air transport erodes quickly. The inherent upfront inefficiencies of air travel (e.g. arriving at the airport early, taxi time, climbing, descent, holding patterns) can take up more time than the actual flight. Additionally, many commercial aircraft are designed to accommodate much longer missions, and therefore, are not optimized for shorter trips. The Hyperloop is a new commercial transportation concept designed to offer both shorter travel times and lower ticket costs for short-haul routes. In order to achieve these reductions, Hyperloop merges a combination of aerospace and ground transportation technologies to achieve a fundamentally new capability. The result is a mode of travel that is maximized both efficiency-wise and environmentally for short missions.

The concept alters the traditional aviation mission profile by bringing the entire trajectory down to the ground level. As a result, a Hyperloop vehicle will not expend extra energy climbing and descending from a cruising altitude and can therefore spend more time operating at cruise conditions. Drag is reduced by flying through a low-pressure tube while conventional wings are replaced by alternative types of lifting bodies (e.g. magnetic and ground effect technologies) that are more compact and have lower induced drag than conventional aerodynamic surfaces. Traveling in a tube also allows the Hyperloop to operate independent of weather conditions and leverage newer and cleaner propulsion technologies.

Since Hyperloop travels in a partial vacuum it must still contend with aerodynamic drag, though the magnitude of that drag is dramatically reduced. The challenge stems from the pressure accumulation as the passenger pod travels through the tube at transonic speed, causing increasing drag over time. To avoid the drag build up, the required tube diameter grows as the pod travel speed increases. At a design speed around Mach 0.8, the required tube size would be on the order of 4 meters in diameter.[1] Travel tubes of this size will contribute substantially to the capital costs for constructing a Hyperloop system. In order to minimize the tube size, Hyperloop can employ an electric compressor in the front of the vehicle to prevent the build up of pressure ahead of the pod. Existing aerospace research for electric aircraft propulsion can be leveraged to provide the necessary technology for this compressor along with recent technological developments in high-density power electronics and power storage. Aerospace modeling techniques also provide better tools

for designing propulsion systems requiring boundary layer ingestion and management.

Staying at ground-level allows the Hyperloop's electromagnetic propulsion system and much of the energy storage system to be located outside of the vehicle. This substantially reduces the weight and mechanical complexity of the individual pods compared to a traditional aircraft that must carry their own propulsion system and 100% of the required mission fuel. There are a number of proposed methods for handling vehicle levitation and propulsion. The original Hyperloop Alpha proposal suggested the use of air-bearings for levitation.[2] Subsequent efforts have focused more on magnetic levitation (MagLev) that can be more tightly coupled to the electromagnetic propulsion system for even higher efficiencies. The concept can be compatible with traditional MagLev systems developed for more conventional high-speed-rail (HSR) applications, but the partially evacuated tube provides an opportunity for even more efficient levitation. The substantially lower drag enables pulse and glide mission profiles, making passive MagLev more viable. This may result in a lighter, more affordable track system, avoiding active levitation components spanning the entire tube length. This unique combination of potential levitation and propulsion technologies differentiate it from previous tube trains and MagLev systems. In the same way an airplane is differentiated from an airship or a hydroplane is differentiated from a boat, the Hyperloop is a plane that generates lift dynamically by moving over a medium at high-speeds rather than depending on buoyancy or static phenomena. The Hyperloop requires a fusion of technologies from both aerospace and HSR applications, though its transonic operation, air-breathing flow-path, and aerodynamically driven design give it qualities more akin to a plane than a train. The constrained, rarefied fluid flow around the vehicle fundamentally alters the design considerations necessary for Hyperloop and requires the consideration of many aerodynamic complexities that are common to aircraft, but not ever seen in train design.

The entire system is held either above ground on concrete columns, underground or underwater within tunnels with the intent of maintaining a relatively straight trajectory. By sacrificing an airplane's traditional mission flexibility, Hyperloop can be optimized for passenger throughput, door-to-door travel time, and energy efficiency for open and level travel corridors spanning highly populous cities. The combination of these technologies allows the vehicle to spend more time operating under optimal conditions and avoids releasing carbon emissions into the upper atmosphere.

The design mission is sized for distances between 250-500 nautical miles, which accounted for 57% of commercial aircraft fleet operations in 2012. NASA's Strategic Implementation Plan stresses that global operations must keep pace with both an overall growing transportation market and simultaneous growth in market share dedicated to air transport. By 2050, 41% of the world traffic (and 71% of North America's) market share is projected to be high-speed transport.[3] This growth will be limited by the existing air-transportation infrastructure and will require dramatic improvements to air-traffic control capabilities to support increased numbers of flights in increasingly more congested air-space.

The Hyperloop offers a compelling opportunity to offset this congestion by offering a faster and lower cost transportation option for a large portion of short-haul aviation routes. Although it requires substantial new infrastructure to be built, numerous high-population adjacent cities exist that have sufficient commercial travel volume to warrant the construction costs. These city pairs are often too far to conveniently travel by car and too short to efficiently travel by plane. Aeronautics market research shows that demand for this travel segment is the most sensitive to technology improvements and ticket price.[4] The departure from typical aircraft constraints is intended to provide a compelling price point considering automobile vehicle miles were estimated to increase by 7 billion simply due to airline fare increases by 10% in 2015.[4]

Beyond the economic benefits of Hyperloop, it offers a significant reduction in carbon emissions. Planes produce large quantities of carbon emissions, exhausted into the upper atmosphere resulting in environmentally damaging travel. The fully-electric Hyperloop is designed for high traffic corridors, where its high upfront cost can be offset by cheaper, faster, and cleaner commercial travel on large scales. The Hyperloop is intended to alleviate billions of commuter car passenger miles, as well as free up airspace, reducing congestion and travel times for flights that are well suited for the national airspace system.

History Aerospace engineers have promoted tube transport for over a century. As early as 1972, a study conducted by the RAND corporation concluded that high-speed 'tubecraft' were technologically feasible, with political pressure being the greatest obstacle to creation.[5] Many concepts later developed by the government, industry, and academia incorporated technologies from which Hyperloop can draw technical precedents. These include, but are not limited to, the Magneplane, Maglifter, and numerous other magnetic propulsion concepts. In 2013, Elon Musk, CEO of Space Exploration Technologies (SpaceX) and Tesla

Motors revived the concept with the Hyperloop Alpha publication.[2] Unlike previous waves of interest, this popularized design has spurred widespread international development efforts amongst leading universities, private companies with over $100M in venture capitalist backing, and smaller research efforts at NASA and the United States Department of Transportation.[1,6]

Focused Research Questions The Hyperloop has largely evolved as an achievable concept over the past several years. In addition to Musk's paper, several key research questions were identified in a study conducted by the Department of Transportation (DOT) to quantify the potential value of the Hyperloop vehicle.[6] This paper works towards answering a few of those key drivers from both an engineering and business perspective.

As highlighted by the DOT, the Hyperloop must be sufficiently lightweight that fixed capital costs of construction, when compared to conventional elevated HSR or MagLev systems, would be greatly decreased. Although true construction costs cannot be estimated through an engineering model alone, this paper seeks to minimize system size, energy, and material quantity as a proxy to cost. This model provides a sensitivity analysis of structural requirements as a function of pod mass to partially answer this research question. Rather than focus on weight of the system explicitly, many of the trends discussed are explored in relation to tube internal cross sectional area. Tube weight relates directly to this area term, and area is the common design variable linking many of the top-level analyses. As depicted in previous work,[1] when abstracting the concept to three top level sizing variables (vehicle frontal area, speed, and tube cross-sectional area) only two are needed to find the third.

Moreover, the potential ability to operate underwater is a key distinguishing feature of the Hyperloop versus conventional HSR and MagLev trains. It is possible for the buoyant force of the submerged tube to counter the systems weight, meaning weight is not a principle factor in this context. Given these considerations, the key research question can be restated as: "Is the Hyperloop sufficiently compact so that there would be construction savings compared to conventional HSR or MagLev systems?" Although you could put a conventional train in an underwater tube, these systems would not be capable of traveling nearly as fast as the Hyperloop in a volume constrained environment. Therefore subsequent results are presented in relation to the tube area.

Another research query, highlighted by the DOT, questions the ability to expand the throughput of the system beyond the 28 passengers per pod originally proposed. This scaling capacity is addressed via analysis of pod frequency combined with design sensitivity to pod length. The relationship between pod mass and number of passengers per pod is also considered in subsequent structural analyses.

The DOT also highlights the need to determine maximum payload capacities of the pods. Adding minimum required weights as model constraints is beyond the scope of this paper, but could be addressed using the engineering methods outlined. Answering this question and better defining component weight breakdowns is recommended as a next step for future work. This paper also does not address land acquisition costs or throughput constraints in today's existing transportation infrastructures. However, the cost modules in this model could consider these constraints if reliable data becomes available in the future. Capacity constrained water ports and airports are critical drivers referenced both in the DOT study and the NASA Aeronautics Strategic Implementation Plan. The prospect of high-speed underwater transportation completely bypasses certain land acquisition challenges and provides a novel solution to eliminating bottlenecks in multimodal travel integration. The analyses performed in this paper are intended to optimize performance based on throughput and cruise conditions. Local transit presents different challenges and objectives than those seen in the longer distances considered in this study. This system model, however, could be easily adapted to perform analysis and optimization of local transit operation in the future.

Paper Scope The paper expands on previous work[1] and the model is built using OpenMDAO, an open-source multidisciplinary analysis and optimization framework written in Python and developed at the NASA Glenn Research Center. This work focuses on balancing the thermodynamic, aerodynamic, structural, weight, and power considerations of the system, with additional calculations for cost and mission design incorporated in the final system. Because each subsystem is designed independently of the whole, this model operates in a modular fashion, providing the flexibility for each subsystem to be replaced with higher fidelity modules in the future. The full model is driven by nested solvers within each subsystem group until all design constraints are met across the entire system. The model is not an attempt to obtain detail design conclusions for the Hyperloop– rather, it is intended to perform sensitivity analyses and trade studies appropriate for evaluating the merit of the concept.

II. Hyperloop System Model Overview

The full-system model of the Hyperloop can be decomposed into two main subsystems: the passenger Pod and Tube. At the top level, these systems are connected to basic cost estimation and notional mission modules. Figures 1 to 3 below describe the structure of this model. The appendix includes an eXtended Design Structure Matrix (XDSM) diagram key, which describes how to interpret the following diagrams for the Pod, Tube, and Mission subsystems.

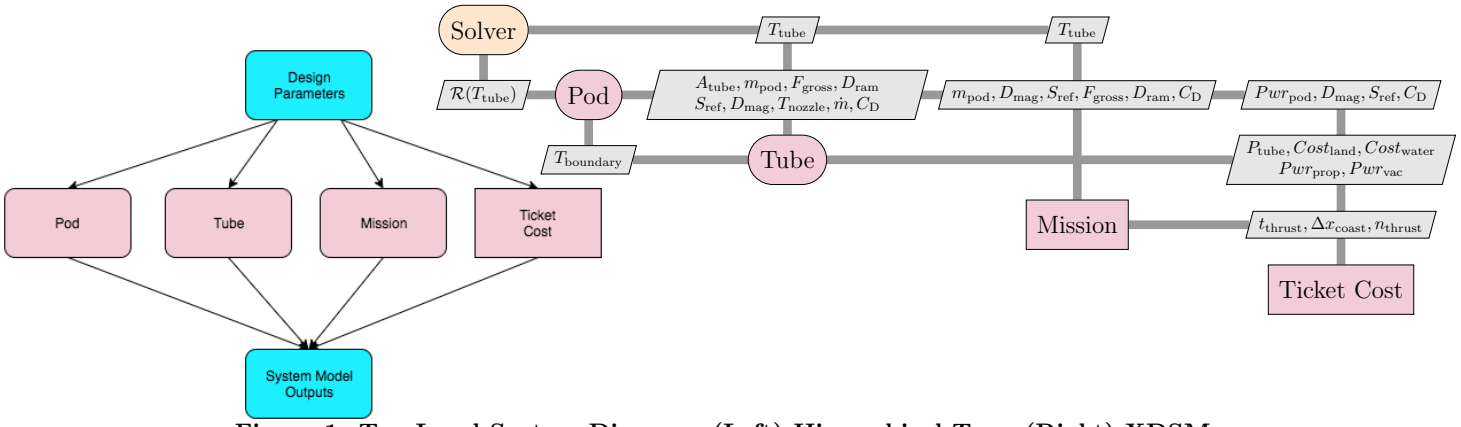

Figure 1: Top Level System Diagram, (Left) Hierarchical Tree, (Right) XDSM

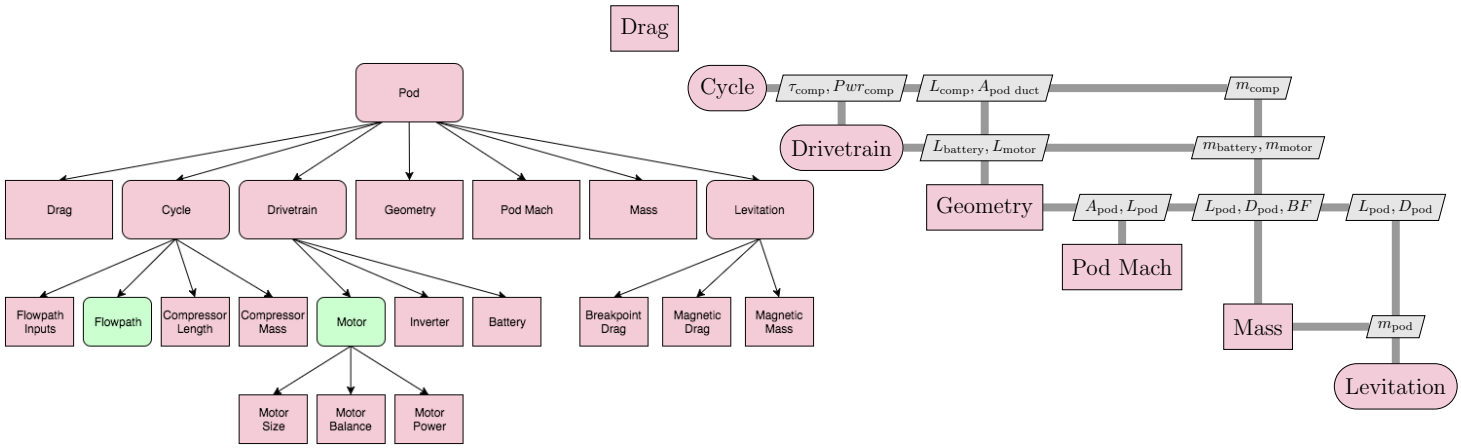

Figure 2: Pod Assembly Diagram, (Left) Hierarchical Tree, (Right) XDSM

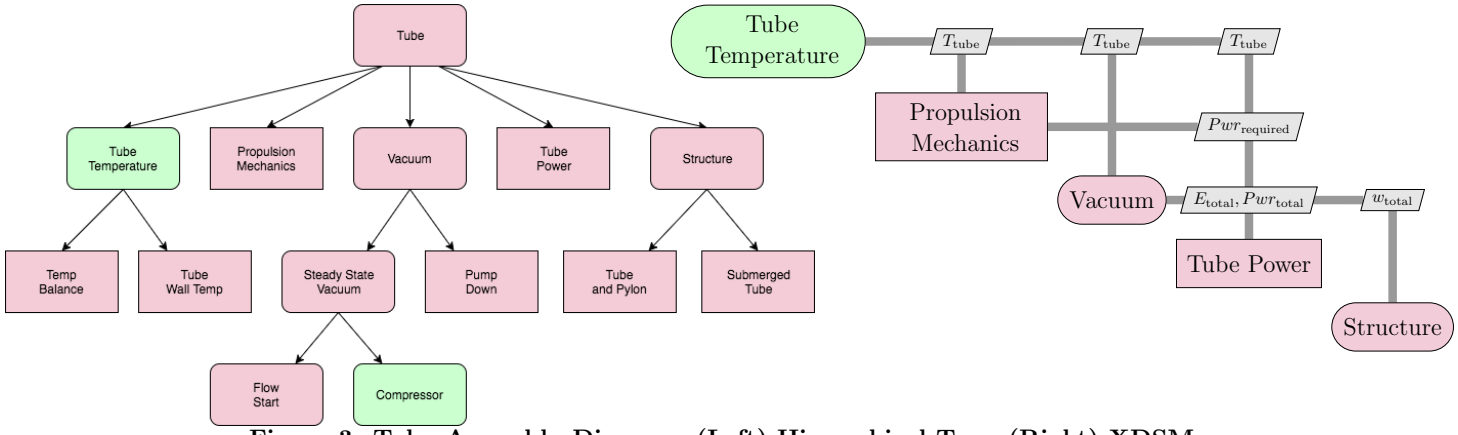

Figure 3: Tube Assembly Diagram, (Left) Hierarchical Tree, (Right) XDSM

Additional levels of subsystems were broken down within the Pod and Tube assemblies. Solver loops exist

at multiple levels within the model, ensuring all design constraints are satisfied across every subcomponent. The XDSM diagrams indicates design variables that are passed from the output of upstream components to be used as inputs for downstream components. Further details can be found in following sections and in the source code documentation, which is referenced in the Appendix.

A. Top Level Component Descriptions

1. Mission

It is necessary to obtain a reasonable estimation of the mission performance requirements in order to carry out system level trade studies. It is important to note that the exact mission route is dependent on the topography of the land between the two notional endpoints. Currently, it is beyond the scope of the model to account for the effect that varying topology will have on the pods trajectory. For simplicity, the model assumes that the pod travels in a straight, flat line between the departure and arrival locations, in this case between Los Angeles (LAX) and San Francisco (SFO) International airports. The mission velocity profile contains three phases: acceleration, coasting with periodic boosting, and deceleration. Figure 4

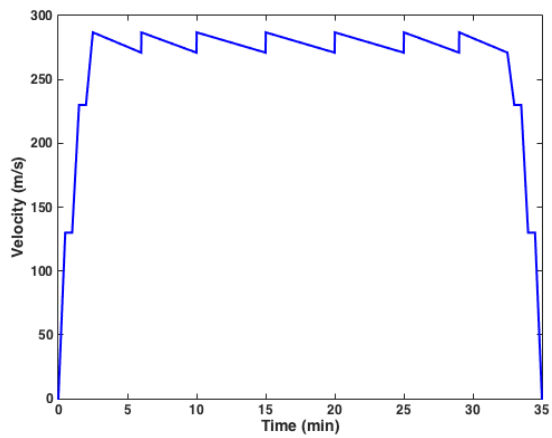

Figure 4: Notional Velocity Profile in Mission Analysis

shows a notional velocity profile using the mission analysis model. The initial acceleration is modeled as a constant linear acceleration of 1g from rest to top speed. Previous analyses have modeled the start up as an incremental acceleration, as is shown in fig. 4, to allow for more maneuverability near departure and arrival points, and to avoid sustaining potentially uncomfortable g forces for prolonged periods of time.[1] The difference in energy consumption between an incremental acceleration and the constant acceleration used in this model is negligible. The second phase of travel consists of a coasting pod with periodic boosting sections. In this phase, the pod begins at top speed and is allowed to coast until it reaches some minimum allowable speed set by the user. Then, the pod will enter an electromagnetic boosting section which will accelerate the pod at 1g back to the desired top speed. For straight and level travel, the acceleration of the pod is given by the equation

$$\frac{\mathrm{d}v}{\mathrm{d}t} = f(v) = \frac{1}{m}(F_{thrust} - \frac{1}{2}C_D \rho V^2 A - D_{mag}) \tag{1}$$

where F_{thrust} is the net thrust generated by the flow through the pod nozzle, C_D is the pod drag coefficient, ρ is the free stream air density, A is the pod planform area, and D_{mag} is the drag produced by the magnetic levitation system. The acceleration equation is integrated to find the time and distance it takes for the pod to decelerate to the minimum allowable speed using a predictor-corrector integration method.

The coast distance is used to determine the number of propulsive sections needed along the track to complete the mission. The energy consumed in a single propulsive section is then multiplied by the number of propulsive sections along the track to determine the electromagnetic propulsive energy consumed per flight during the coasting phase of the mission. The final phase of the mission is a constant linear deceleration of 0.5g from top speed to rest. Many systems driven by electromagnetic propulsion conserve energy through regenerative braking.[7] For the sake of conservatism, it is assumed that there is no regenerative braking in

this process, although the model allows for regenerative braking to be accounted for if the user desires. The energy consumed per flight is computed by adding the consumption of all three phases.

2. Cost

The cost module estimates the cost of energy, materials, pods, and construction capital. The cost of construction is highly subjective and it is difficult to get an accurate estimation within less than an order of magnitude of uncertainty. However, the cost of materials and energy consumption can be estimated with significantly greater certainty. Thus, in this analysis, the cost estimations of materials and energy are of greater interest. The average price of electricity used in the model is 0.13 USD/kWh, based on data from the Electricity Information Administration.[8] Using a different value will not significantly change the trends in the trade studies this model produces. A rough estimation of the ticket cost is included, which projects ticket cost based on the equation

$$\mathrm{Cost}_{\mathrm{ticket}} = \frac{(\frac{\partial \mathrm{Cost}}{\partial D} D + \frac{\partial \mathrm{Cost}}{\partial \mathrm{pod}} n_{\mathrm{pods}} + \mathrm{Cost}_{\mathrm{capital}}(1+ib) + \frac{\partial \mathrm{Cost}}{\partial \mathcal{E}}(\mathcal{E}_{\mathrm{tube}} + \mathcal{E}_{\mathrm{pod}})))}{n_{\mathrm{passengers}} * \frac{\mathrm{pods}}{s} * 3600 \frac{s}{\mathrm{year}} * 24 \frac{\mathrm{year}}{\mathrm{day}} * 365 \frac{\mathrm{day}}{\mathrm{year}} * bm} \tag{2}$$

Where ib is the bond interest rate, bm is the number of years for bond maturity, and D is the total length of the track. Previous research indicated that construction costs are likely to be the largest cost factor in the system.[2] Due to the lack of a reliable method of estimating construction cost or ticket markup at this stage of the design process, the exact values of the ticket cost produced by this model will have a high level of uncertainty. However, the trade studies conducted in these analyses can provide useful information to inform the development of more accurate ticket cost models in the future.

B. Pod Level Component Descriptions

The design of the tube is driven by the configuration of the pod. Consequently, the system model is constructed such that the pod design is analyzed first. The Pod group contains all subsystems onboard the passenger pod. The module takes in design variables and feeds them into the Drag, Cycle, Drivetrain, Geometry, Mass, and Levitation subsystems.

1. Drag

Computational Fluid Dynamics (CFD) was performed on the pod to determine how the pod drag coefficient varies with Mach number. Pod aerodynamics were computed with the Fully Unstructured Navier-Stokes 3D (FUN3D) flow solver.[9] FUN3D is a node-based computational fluid dynamics code for mixed element types that uses a second-order accurate point-implicit method for numerical convergence. The upwind inviscid flux difference splitting scheme of Roe[10] was used to compute cell interface fluxes, with turbulence closure obtained using the one equation model of Spalart and Allmaras.[11] All computational boundaries were discretized using the Glyph scripting language of the commercial mesh software Pointwise. Volume discretizations were generated from the surface domains using the advancing-front local reconnection (AFLR3)[12] algorithm. For computational efficiency, extruded viscous prism layers were generated near the pod surfaces and transitioned to isotropic tetrahedral cells outside the boundary layer region. All viscous cells were resolved to a $y^+ < 1$. Volume meshes for the core domain contained approximately 19 million cells.

The computational domain is depicted in Figure 5a, and modeled assuming vehicle half-symmetry. The tube was simulated thirty vehicle body lengths upstream of the pod and extended one hundred body lengths downstream. Boundary conditions were applied on all computational domains. A freestream condition enforcing Mach number and static air reference properties was specified at the tube inflow boundary. A uniform static backpressure was specified on the tube downstream exit. An inviscid boundary condition was prescribed on the tube walls to avoid the formation of a viscous boundary layer. All surfaces of the pod were assigned a viscous no-slip condition, except flow-through domains where compressor and nozzle boundary conditions were applied. At the compressor fan face, a uniform static back-pressure was prescribed. At the nozzle plenum, total temperature and pressure ratios with respect to freestream were specified.

Drag coefficients, non-dimensionalized by pod planform area, were extracted from simulation results. Drag forces included only viscous and pressure forces acting on external pod surfaces and excluded ram and internal nozzle drag effects.

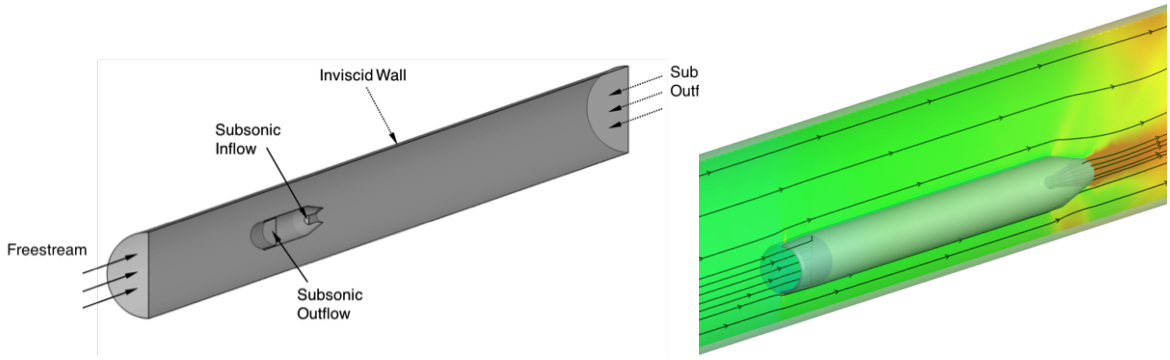

(a) Computational boundary applied to vehicle flow domain. **(b) Resulting Flow Contour**

Figure 5: CFD model

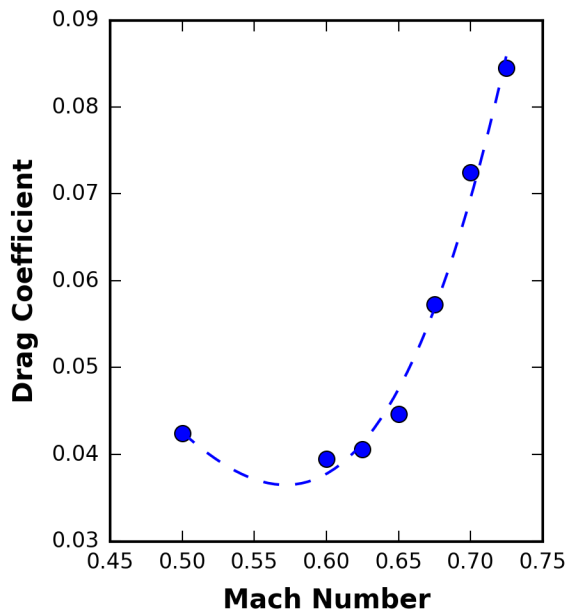

Figure 6: Drag Coefficient vs. Mach Number

Figure 6 shows the CFD results for drag coefficient vs. Mach number. These results fit the trend expected for transonic flow given by the Prandtl-Glauert relationship. Drag coefficient values were then interpolated from this data for each Mach number the system analyzed.

2. Cycle

The on-board compression system provides a means of increasing the maximum pod speed over a closed pod, and provides a small amount of thrust. A thermodynamic analysis of the compressor system is necessary to estimate on-board power requirements and overall heat rise of each pod. The compression cycle is comprised of an inlet, compressor, duct, nozzle, and shaft that is connected to the electric motor drivetrain. The design deviates from the original Hyperloop proposal by removing two heat exchangers as well as the air-bearings. The system is modeled as a one-dimensional cycle, representing components as thermodynamic processes that are subsequently chained together. Each component is responsible for calculating gas properties across its boundaries and appropriately enforcing conservation equations across the entire system. This model builds off the NASA Glenn developed PyCycle framework, which is a thermodynamic modeling framework developed in Python with the capability for optimization employing analytic gradients.[13]

3. Drivetrain

The Drivetrain module models an electric motor, inverter, and battery system by computing the size and mass of both the motor and battery system required to sustain the torque and power demands over a mission profile.[14,15] The model modifies an existing algorithm developed at NASA for battery sizing by utilizing a spline fit of voltage discharge curves provided by battery manufacturers to compute voltage as a function of discharge instead of the generic physics-based model used in previous work.[15] This change provides results that are more flexible and specific to the leading commercial battery cells.

4. Geometry and Mass

In order to analyze the design of the tube structure, the final mass and geometric configuration of the pod must be obtained. The Geometry model assumes the pod to have a cylindrical fuselage with conical frustums at the inlet and exit. The cross sectional area of the passenger section given by the user is added to the cross sectional area of the compressor exit duct, which is computed in the cycle analysis. The Geometry module also estimates the thickness of the pod wall and the passenger compartment based on simple pressurized cylinder relationships. It then adds these areas together to compute the total cross sectional area. The length of each component is also fed into the Geometry model so it can compute the total pod length and planform area. The Mass module takes the mass of each component and adds them with the total passenger mass in order to determine the mass of the pod, without magnets, for levitation. The Levitation component takes in this mass, computes the mass of the magnets, then outputs the total mass of the pods.

5. Pod Mach

The Pod Mach module uses the pod cross-sectional area, Mach number, and compressor inlet conditions to compute the tube area. As the pod travels, flow that is not entrained by the compressor must accelerate around the pod. Due to the pods transonic flight speed, it is possible that this bypass flow could accelerate to Mach 1 and cause the flow to choke, which would lead to an undesirable buildup of pressure in front of the pod and increased drag. To avoid this condition, this module sizes the tube area such that there is a large enough bypass area to prevent the bypass flow from accelerating to Mach 1. This is done using a simple quasi 1D area relationship for compressible flow given by the equation

$$\frac{A_1}{A_2} = \frac{M_2}{M_1}\left(\frac{1+\frac{\gamma-1}{2}M_1^2}{1+\frac{\gamma-1}{2}M_2^2}\right)^{\frac{(\gamma+1)}{2(\gamma-1)}} \tag{3}$$

For this analysis, M_1 is the free stream Mach number, M_2 is the desired bypass Mach number, A_1 is the initial area of the bypass flow (A_{tube} - A_{inlet}), and A_2 is the bypass area (A_{tube} - A_{pod}). For these analyses, M_2 is set to .95 in order to provide a slight factor of safety to prevent the flow from reaching the choking condition. In order to make this model higher fidelity, it is possible to modify the areas in the relationship to account for boundary layer development over the pod's outer surface. As the boundary develops, the effective bypass area is reduced which increases the risk of bypass flow reaching Mach 1. However, it is possible to modify this by increasing the effective pod radius by the displacement thickness of the boundary layer. The sensitivity of structural design to boundary layer growth is important and will be discussed at length later.

6. Levitation

The Levitation group makes two critical calculations: the inductance of the track required for the pod to levitate at a desired speed and the mass of the permanent magnets located onboard. The Breakpoint Levitation module employs a desired minimum levitation speed and uses it to calculate important track parameters, including the ratio of inductance to resistance of the track.

The pod levitation system is designed to significantly reduce friction during high velocity travel. In this analysis, a passive magnetic levitation system is used to suspend the pod above the track. A passive system is advantageous because it requires zero power input for levitation to occur at a given speed. Magnetic drag is still present, however pod speed is replenished during each boost phase as depicted in the mission discussion. Track cost accounting is not included in the model, but this configuration was chosen to reduce overall track requirements to essentially metal strips configured to maximize conductivity and minimize eddy current

generation. The Halbach array passive levitation method developed at the Lawrence Livermore National Laboratory is chosen as the baseline system for modeling MagLev performance.[7] It is assumed that ferrite tiles were not used so that the added inductive loading is set to zero, leaving only the distributed inductance to compute in the model. Fringe fields from the magnetic array are also ignored in this analysis and the width of the magnetic array is set equal to the width of the track. These three simplifications reduce the parameters needed to determine magnetic lift force to $\beta,_{mag}, \lambda, R, L, A$, which are magnetic strength, width, wavelength, equivalent circuit resistance, inductance, and area as shown in eq. (4).

$$L_{mag} = F_y(\omega) = \frac{\beta_0^2 w_{mag}\lambda}{4\pi L d_c}\frac{1}{(1+R/\omega L)^2}A_a e^{-4\pi h/\lambda} \ , \tag{4}$$

Using the desired levitation speed, the total mass of magnets required and drag force produced is then calculated. The drag produced by the magnets are given in eq. (5)

$$D_{mag} = (m_{pod}g)R/\omega L \tag{5}$$

In these equations, the drag and the magnet mass are both functions of the magnet area and thickness. To minimize drag and mass, a Pareto front is quantified prior to running the system model. The following cost function is developed by normalizing drag and mass, then multiplying by a weighting factor *alpha* and adding them together in the following equation

$$f(\alpha) = \alpha\bar{F_x} + (1-\alpha)\bar{m_{mag}}v \tag{6}$$

Where the bar signifies the normalized value. The weighting factor *alpha* is chosen arbitrarily between zero and unity; high values of *alpha* emphasize minimizing drag while low values of *alpha* emphasize minimizing mass.

C. Tube Level Component Descriptions

Once the Pod group determines the design configuration of the pod, the dimensions are fed into the Tube group. This group contains the subsystem analyses for the vacuum pumps, electromagnetic propulsion system, thermal management, and tube structure. Once the major aspects of the design of the tube are evaluated, results for both Pod and Tube design can be fed into Mission and Cost analyses to evaluate overall system performance requirements and their resulting costs.

1. Vacuum

The vacuum subsystem is a group that evaluates two different operations: pump down and steady-state usage. The pump down module evaluates the number of vacuum pumps and the energy required to drop the pressure from ambient to the operating condition. This information is critical because the vacuum will need to be pumped down once the tube is constructed and in the event of an emergency pressurization. The energy required to draw down the tube pressure is given in the equation

$$E_{tot} = pwr * \frac{vol_{tube} * speed_{pump} * log(P_0/P_f) * 2}{t_{pumpdown}} * u_P * 86400\frac{sec}{day} \tag{7}$$

The energy usage for this operation will be a critical element of operating cost. The pump down operation is only the first step in getting the travel tube down to operational pressure. Once that is done, we enter a steady-state phase. In theory, if the tube is perfectly air tight, there would be no need for the vacuum to run at all once the tube is pumped down. However, air is likely to leak into the system throughout normal operation, particularly during the loading of pods into the tube. Consequently, vacuum pumps will need to be used throughout operation to maintain operating pressure. The effect of leakage rate on energy consumption is critical and will be discussed in more depth later. For the purpose of this analysis, the steady-state vacuum pump is modeled as a compressor using the same type of thermodynamic model employed in the pod cycle analysis. The pressure ratio of the vacuum will be equal to the ratio of ambient pressure to desired tube pressure and the mass flow through the vacuum at steady state will be equal to the leakage rate.

2. Thermal Management

A basic heat balance is performed to determine the approximate tube temperature. The quasi-steady analysis ignores heat transfer time lags and diurnal cycles. Heat is assumed to transfer and equilibrate rapidly between the pod compressor system, the rarified atmosphere inside the tube, the tube walls, and the outside environment. This analysis is based off previous work by Chin et al.[1] and concludes manageable heat loads for air-cabin cooling. A conservative equilibrium tube temperature, with the tube in direct sunlight, on a 90 degree Fahrenheit hot day and during maximum pod operation, is on the order of 110 degrees Fahrenheit. For an underground or underwater trajectory, these estimates would drop even lower.

3. Electromagnetic Propulsion

A series of linear synchronous motors (LSMs) is proposed to accelerate the pod from rest to top speed and maintain top speed with periodic boosts. While the specifications of the LSM system design are beyond the scope of this analysis, the amount of energy and power required of an LSM can be determined using the simple mechanics relationship,

$$F_{net} = F_{LSM} + F_{thrust} - \frac{1}{2}C_D \rho V^2 A - D_{mag} \tag{8}$$

in which F_{LSM} is the force required of the LSM system. This equation is integrated to determine the power and energy requirements for both startup and coasting booster sections. For the purpose of this analysis, the efficiency of the LSM is assumed to be 0.8 based on rough approximations.[16]

4. Structure

The Structural group determines the structural design of the tube for two phases of travel: travel over land and under water. When traveling overland, the tube is assumed to be supported by pylons above the terrain at a given height. For travel under water, the tube is notionally supported at a certain depth below sea level. The structural analysis in each phase is under constrained and allows for several free choices to be made by the user, which could have a significant impact on design configuration and material cost. To handle this challenge, the structural design of the tube at each phase was optimized in order to determine the configuration that minimizes cost. The optimization methods will be discussed later in further detail.

III. Subsystem Analyses and Optimizations

Before conducting top-level trade studies, individual subsystems were analyzed. Multiple subsystems have key parameters that required reasonable values before the fully integrated model could return reasonable results. Prior to running trade studies, optimizations are performed in order to select values for any of the unknown inputs. The methodology used to perform these optimizations is discussed in detail in this section. Furthermore, analyses of individual subsystems can provide critical insight into system level behavior. The variations in energy consumption, structural costs, and capacity scaling can be initially observed through these subsystem analyses, then more fully developed through system level analyses. Subsystem analyses that provide critical insight to system level behavior are discussed in this section as they begin to illustrate major conclusions.

A. Structural Subsystem Optimization

A structural analysis is performed on the tube for multiple geographical scenarios, as the pod travels both over land and under water. In these analyses, material properties of steel and concrete are used for the tube in order to illustrate trends. Both phases are analyzed prior to running the full system using values of design variables suggested from previous research with safety factors where appropriate.[1] Then, cost function optimizations are performed with appropriate design variables to determine which input values minimize material cost. These values will then be fed into the whole system model to perform trade studies on top-level design variables. It is understood that the values obtained by performing optimization on subsystems will likely not be optimal when the whole system is analyzed; however, these values are useful for illustrating physical trends and system trades. The ScipyOptimizer is used to minimize the scalar cost function using the Sequential Least Squares Programming (SLSQP) algorithm for gradient-based optimization.[17,18]

First, travel of the pod over land is analyzed. In this case, the pod travels within a tube that is suspended on pylons of a given height above the ground. To perform this analysis, multiple simplifying assumptions were made. The tube is assumed to have thin walls relative to the tube radius and thus will be modeled as a thin-walled pressure vessel. The tube is assumed to be horizontal and the height of the pylons is assumed to be constant for simplicity. This allows a section of the tube between two pylons to be modeled as a hollow cylindrical beam with simple supports at its ends. Each pylon is modeled as a beam fixed at the ground with axial and transverse loads applied to its end. The structure is designed according to beam bending equations with the sectional weight of the beam modeled as a distributed load and the mass of the pod as a point load at the beams center. The structure is analyzed with the pod at the center of the beam since this produces the highest bending stress scenario. With these assumptions, two extreme structural configurations can be imagined: one in which the tube is thick, but is supported by pylons that are spaced very far apart, and another in which the tube is thin, but must be supported by many closely spaced pylons. A cost function is developed by adding the cost of the tube material and the cost of the supporting pylons per unit length, with the thickness of the tube and the distance between pylons as design variables as shown in eq. (9) below,

$$\frac{\text{Cost}}{\text{Length}} = \frac{TubeCost}{kg} * m'_{\text{pod}} + \frac{\text{Pylon Cost}}{kg} \frac{m_{\text{pylon}}}{\Delta x_{\text{pylon}}} \tag{9}$$

where m is the mass per unit length of the tube. This model, however, is incomplete because the pylons can be any arbitrary size. To fix this issue, the pylons are sized according to the buckling condition for a fixed column. Imposing this condition allows for the spacing of the pylons to be computed in terms of pylon radius and tube thickness using eq. (10)

$$\Delta x_{pylons} = \frac{\frac{\pi^2 E r_p^4}{16h^2} - \frac{1}{2} m_{pod} g}{\frac{1}{2} m' g} \tag{10}$$

Using this relationship, the cost function is defined with the tube thickness and pylon radius as design variables. The final step is to appropriately constrain the optimization. The minimum radius of the pylon is computed based on the yield strength of the pylon material. Likewise, the minimum thickness of the tube is calculated using the buckling condition for vacuum cylinders given by eq. (11)[19]

$$P_{crit} = \frac{\gamma E}{4(1-\nu^2)} (\frac{t}{r})^3 \tag{11}$$

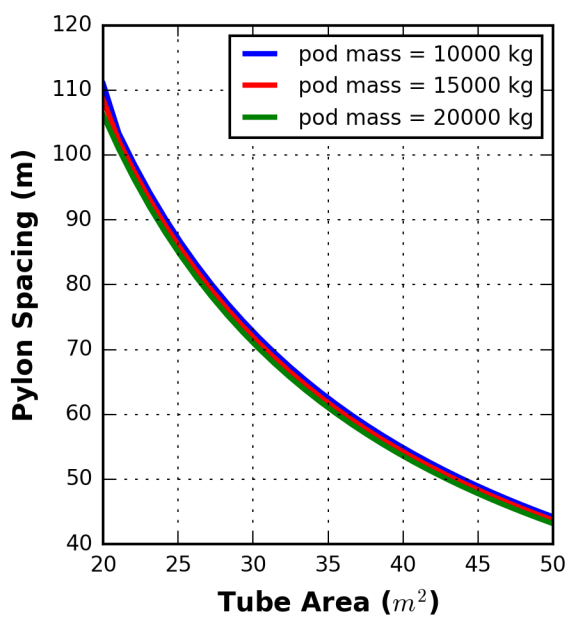

Figure 7: Optimal Pylon Spacing vs. Tube Area

For this analysis, the area of the tube is varied and the pylon spacing is recorded for different pod masses. Figure 7 shows that pylon spacing decreases significantly as tube area increases. This is a reasonable result since, as tube area increases and becomes heavier, larger pylons are needed to support the heavier load and a thicker tube is needed to handle higher bending stress, both of which increase cost. This optimization shows that moving the pylons closer together mitigates this cost penalty. When analyzing the top level of the entire system, Figure 7, along with the pylon buckling constraint, will be used to determine reasonable inputs for tube thickness and pylon spacing for any given tube area or pod mass. This is done in order to reflect optimal structural design conditions as closely as possible. These results also give us preliminary insight into how favorably the Hyperloop structure scales with pod capacity. For any given tube area in this regime, increasing the pod mass from 10,000 kg to 20,000 kg results in a change in pylon spacing of less than 2%, with the sensitivity of pylon spacing to pod mass decreasing for higher tube areas. This suggests that the mass of the tube is dominant when sizing the structure of the system and that the pod mass is negligible at this design point. This means that the capacity of each pod can be increased with negligible ramifications on structural design. Pod capacity trades will be discussed in greater detail in the following sections. However, this analysis shows that pod capacity can be greatly scaled up with minimal impact on structural design or the cost of materials and construction. A structural analysis is also performed for underwater travel. The model will have to be altered slightly from the model of the pod over land in order to account for buoyancy. In this case, a section of the tube is modeled as a hollow cylindrical beam subjected to a distributed load equal to the difference between the sectional buoyancy and the sectional weight. Travel underwater could have an interesting effect on structural design because it is possible for the tube to be sized such that the entire weight of the structure is suspended by its own buoyancy. In this case, supporting structure would only be necessary to stabilize the structure against changing tides, currents, and seismic activity rather than supporting the structural load. Figure 8 shows the tube thickness at which the buoyant force is equal to the weight of the tube allowing the tube structure to support itself. Points above this curve will have weight greater than buoyancy and thus will require pylons to support the weight. Likewise, points below this curve will result in a buoyant force that is greater than the weight of the tube and would require structures to anchor the tube at a certain depth.

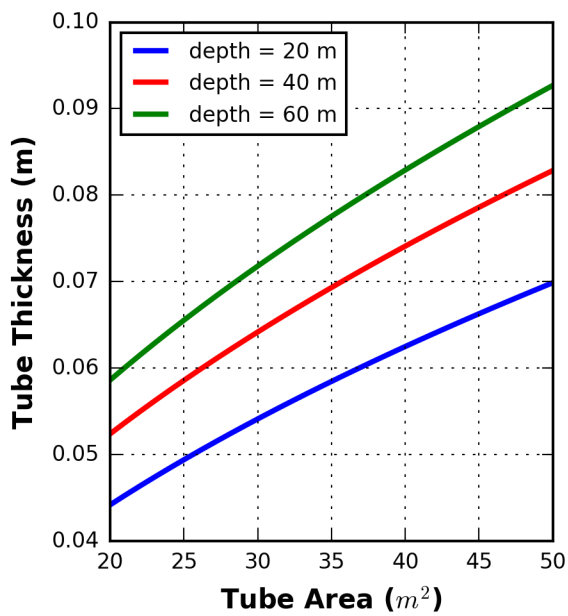

Figure 8: Tube Thickness vs. Tube Area of Travel Under Water

Traveling under water, unlike over land, allows the ambient pressure to change significantly with the depth. Figure 8 shows the sensitivity of tube thickness to tube area for multiple different values of depth. For large depths, thickness increases with tube area at a faster rate, which results in increased material cost. It is important to note that the thickness values calculated in this analysis are significantly below the values necessary for self-suspension given in fig. 8. Thus, for underwater phases, it can be concluded that the

Hyperloop structure would likely be subjected to a buoyant force greater than the weight of the system and would need to be designed in such a way that the tube is anchored to the sea floor and stabilized in the event of disturbances. The structural trade studies shown here suggest that there could be significant benefits to traveling underwater as opposed to over land. The depth could be chosen such that the tube could be thinner. Furthermore, it will likely be easier to make a straighter path traveling underwater because there will be obstructions to contend with. Since the tube needs to be air-tight, regardless of whether travel is underwater or overland, either phase will likely require similar levels of manufacturing cost. Underwater tunneling may pose larger costs and challenges associated with installation and maintenance, but will substantially reduce land acquisition costs. While evaluating the exact cost differential is beyond the scope of this paper, due to the very coarse cost analyses used, this system model suggests that there could be substantial benefits from traveling underwater and should be the subject of further research.

B. Pod Frequency

The traffic between the notional end points and the market demand for tickets at a given cost will determine the amount of passengers the Hyperloop must be able to accommodate in a given period of time. The number of passengers per unit of time that the Hyperloop can transport is equal to the number of passengers per pod times the frequency at which pods depart. If a constant pod capacity is assumed, then the only way to accommodate periods of high demand is to increase the frequency at which pods depart. It is important to understand the limitations of pod frequency in order to obtain a reasonable sense of maximum passenger throughput. There are three factors that must be considered when evaluating limitations on pod frequency: safety, the amount of time it takes to board, and the number of pods available. Pods must be spaced out such that each pod can slow down and stop before hitting the pod in front of it in the event of an emergency stop. Linear acceleration equations can be used to determine the minimum distance separation diatance to allow for deceleration. This analysis determined that pods would need 30 seconds to decelerate at 1 g to avoid collision, which corresponds to a maximum pod frequency of roughly 2 pods per minute. These calculations can be found in the source code referenced in the Appendix. This frequency should easily be satisfied, even with a safety margin, due to the time that must be allowed for passengers to board. It is likely that passengers will need considerably more than 30 seconds to board, meaning that safety will most likely not be the limiting factor on maximum pod frequency. Finally, in this analysis, it is assumed that the operator must have enough pods to fill the entire tube when launching flights at a given frequency. Consequently, having less time in between pods reduces the distance in between pods, which increases the number of pods required to fill the tube and sustain the desired pod frequency. Due to these three limiting factors, lower pod frequencies are desirable because they increase the safety margin in the event of emergency braking, increase the time passengers have to board, and reduce the number of pods that the operator must have in order to sustain a given pod frequency. The impact of changes in pod capacity on system design and performance will be discussed in further detail later in this study.

C. Boundary Layer Sensitivity

In the system model, the tube cross section is sized such that the flow in the pod does not choke. Previous models have attempted to impose this condition by assuming that the area of the bypass flow is equal to the tube cross sectional area minus the pod cross sectional area.[1] This model attempts to build upon previous models by also accounting for the development of a boundary layer over pod surface. The boundary layer formation further reduces the bypass area and increases the chance of choking in the flow. Thus, a larger tube will be necessary to prevent choking when boundary layer effects are accounted for, which will increase the costs of both raw materials and construction. This model will first analyze the sensitivity of the tube cross sectional area to the boundary layer growth along the pod surface. Then, estimations of boundary layer thickness as a function of length-based Re will be made in order to analyze the sensitivity of tube cross sectional area to changes in pod length. For each analysis, the tube is sized using the previously discussed inviscid, quasi-1D area relationships for compressible flow. To account for the boundary layer using this method, the boundary layer is modeled as a cylindrical ring with a thickness equal to the maximum thickness of the displacement boundary layer, δ^*, over the outside of the pod, effectively reducing the area of the bypass flow. Using this model, the contraction of the bypass flow is given by eq. (12)

$$\frac{A_{\text{bypass eff}}}{A_{\text{bypass}}} = \frac{A_{\text{tube}} - A_{\text{pod}} - \pi((r+\delta^*)^2 - r^2)}{A_{\text{tube}} - A_{\text{inlet}}} \tag{12}$$

This relationship accounts for the reduction in bypass area due to a boundary layer of arbitrary displacement thickness. First, the sensitivity of tube area to displacement boundary layer thickness is studied over a range of boundary layer thicknesses for various pod cross sections. Next, the model uses a flat plate approximation to obtain a relationship between boundary layer and length. Since $Re > 500,000$, the boundary layer is assumed turbulent with a velocity profile[20]

$$\frac{u}{U} = (\frac{y}{\delta})^{1/7} \tag{13}$$

Using this boundary layer velocity profile, the thickness of the displacement boundary layer is derived using a similarity solution to produce the equation[20]

$$\frac{\delta^*}{x} \approx \frac{.04775}{Re_x^{1/5}} \tag{14}$$

The system model uses eq. (14) to relate displacement boundary layer thickness, and therefore tube area, with pod length. These equations do not perfectly represent real physical relationships as they are derived from Fox and McDonald assuming 1D flow over a flat plate with zero pressure gradient. Characterizing the displacement thickness of the boundary layer in 3D conical flow is beyond the scope of this analysis. However, the approximation made in this analysis is useful for studying how tube area and material costs may change with increasing pod length within an order of magnitude of accuracy. The pod configurations tested in each analysis are given in Figure 9. These two charts show the same data presented in slightly different ways. Figure 9a shows how the required tube area varies the maximum δ^*. δ^* grows as the pod gets longer, so Figure 9b presents the same data as a function of pod length.

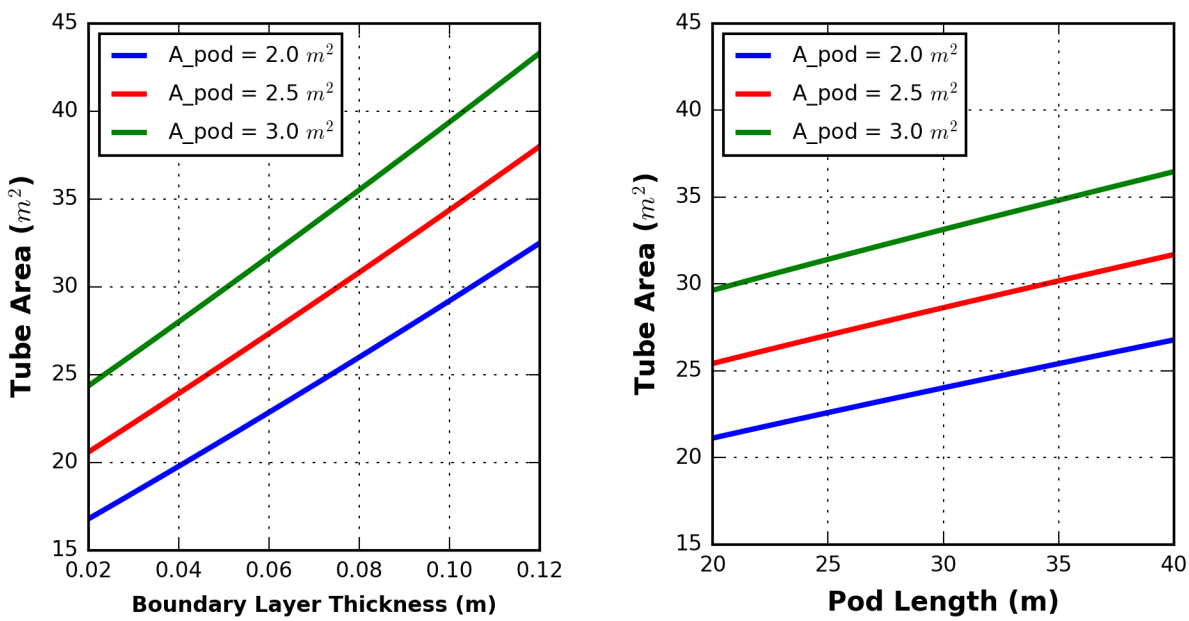

(a) Tube Area vs. Boundary Layer Thickness for Multiple Pod Areas **(b) Tube Area vs. Pod Length for Multiple Pod Areas**

Figure 9: Tube Cross Sectional Area Sensitivity

For $A_{pod} = 2\,\mathrm{m}^2$, a 1 cm increase in δ^* results in an increase of approximately $1.57\,\mathrm{m}^2$ in A_{tube}. Thus, it can be concluded that the tube area, and therefore the tube material cost, are extremely sensitive to boundary layer thickness. Furthermore, the rate of increase of the tube cross sectional area also increases with pod cross sectional area. This relationship exists because more bypass area is lost as the pod radius increases for a given displacement boundary layer thickness. This means that the coupling between tube and pod cross sectional areas is even stronger than was indicated in previous research.

Figure 9b shows the necessary cross sectional area of the tube as a function of pod length using the previously described relationship approximation. Increases in pod length due to higher passenger capacity,

increased battery length, more compressor stages, etc., require the tube cross sectional area to increase in order to accommodate for larger boundary layer growth. Due to the sensitivity of tube area with respect to boundary layer thickness, it is important to develop a model that can accurately determine the displacement boundary layer thickness over the pod surface in order to avoid undesired choking or the development of shock waves in the tube. Moreover, this analysis suggests that active flow control techniques, such as boundary layer suction, which reduce boundary layer thickness, could be very beneficial.

The sensitivity of tube area with respect to pod length has interesting implications on how the material cost of the tube scales with passenger capacity. As pod capacity increases, the passenger compartment of the pod must increase to accommodate more people. The cross sectional area of the tube is too sensitive to the cross sectional area of the pod to allow for any undue increase, so the pod length must be extended to account for higher capacity. However, increasing pod length does have a non-negligible effect on the tube cross sectional area when boundary layer development is considered. Therefore, it is even more important for future iterations of this system model to include higher fidelity boundary layer modeling. This could also make the infusion of active flow control aboard the pod even more compelling. Boundary layer growth will be accounted for using these methods in a discussion of passenger capacity trades later in this study.

IV. Results

A. Mach Number Trades

The cost of the pod infrastructure is highly coupled with the Mach number at which the vehicle travels. In order to obey the choking constraint, higher Mach numbers will necessitate a larger tube to prevent the flow around the pod from accelerating to the speed of sound. This increases the material cost of the tube and the energy required to pump down the tube. In this analysis, the full system model will be run for a range of Mach numbers. For each Mach number, the area of the tube is recorded along with the total energy cost. In this analysis, the leakage rate is assumed to be a constant mass flow on the order 1 kg/s. This value should be sufficient for illustrating the trend of energy consumption as a function of Mach number. Different values of leakage rate will not significantly alter the trend, but will instead directly scale the amount of energy used by the vacuum system in a steady state condition. Figure 10 indicates how the tube area and energy

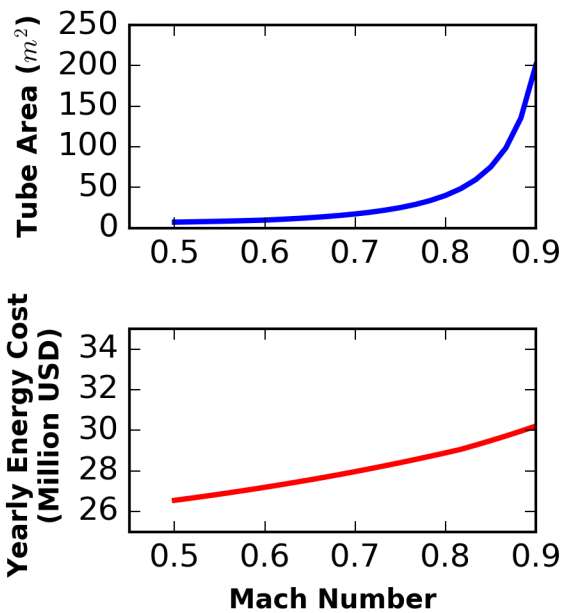

Figure 10: Tube Area and Yearly Energy Cost vs. Mach Number

consumption change over a range of Mach numbers. As is indicated in previous research, tube area begins to increase rapidly around Mach 0.8.[1] Beyond this Mach number, small increases in Mach number result in a large increase in tube area, which will have a large impact on capital cost and energy consumption

during pump down. Conversely, fig. 10 indicates that tube area, and therfore material cost, grows slowly with Mach number for Mach numbers below 0.8. Based on these results, it is estimated that any system level optimization of cost with respect to Mach number will likely result in a Mach number near 0.8. For this reason, a Mach number of 0.8 will be used in subsequent analyses to obtain reasonable evaluations of design trades and system behavior.

B. Pressure Trades

One of the most critical design variables of the Hyperloop is the tube pressure at which it operates. A lower pressure increases the power required of the vacuum system in order to pump the tube down and maintain tube pressure for a given leakage rate. However, operating at a higher pressure will increase the density of the air and thus increase the power requirements of both the electromagnetic propulsion system and the onboard compressor. As compressor power requirements change, the length and mass of the motor and battery will change the pod geometry. Tube area is coupled with pod length, as was shown in the boundary layer analysis, while the power required of the electromagnetic propulsion system is coupled with pod mass. The boundary layer that was described previously is used for this analysis. Tube pressure is perhaps the single most important design variable to understand, because it is coupled with so many different aspects of system construction and performance. Trade studies using this fully comprehensive system model can provide valuable insight into the effects that variations in pressure have in every aspect of design and performance at the system level. Previous research has suggested that the ideal operating pressure should be on the order of 100 Pa.[1,2] However, such a low pressure could be costly and difficult to implement across a larger stretch of tube, especially if there is significant leakage. It is likely that slight increases in tube pressure could result in significant decreases in energy consumption that could make up for increased drag penalty. To evaluate this, the full system model was run for a range of pressures. Tube area, compressor power, steady state vacuum power, and total yearly energy consumption are recorded at each pressure.

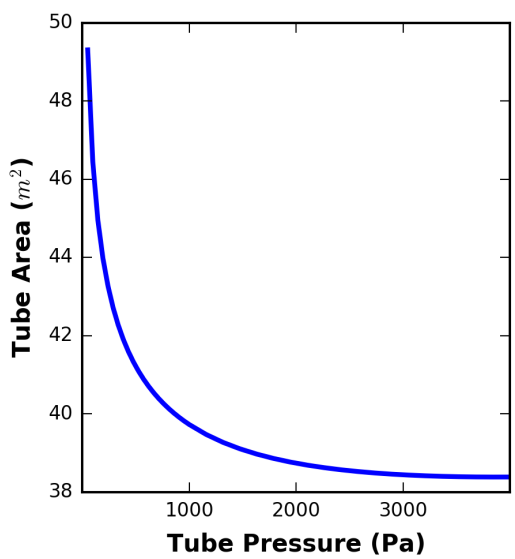

Figure 11: Tube Area vs. Tube Pressure

Figure 11 shows tube area as a function of tube pressure. As pressure increases, tube area decreases until leveling off around 3500 Pa. This relationship is due to the effect that pressure has on boundary layer thickness. Increasing the pressure increases the Reynolds number per unit length, which decreases boundary layer thickness. As boundary layer thickness is reduced, the effective bypass area is increased which allows the tube area to be reduced for the same Mach number. However, compressor power increases linearly with pressure, which results in an increase in pod length to hold a larger motor and battery. As was shown previously, increasing length results in increased boundary layer growth and causes tube size to grow. This trade off, illustrated in fig. 11, results in two distinct trends. At lower pressures, marginal increases in pressure result in decreases in tube area because the increase in Reynolds number per unit length dominates the length increases necessitated by higher compressor power demands. Meanwhile, at higher pressures,

increases in pod length begin to dominate boundary layer sizing and the marginal effect on tube area is tempered.

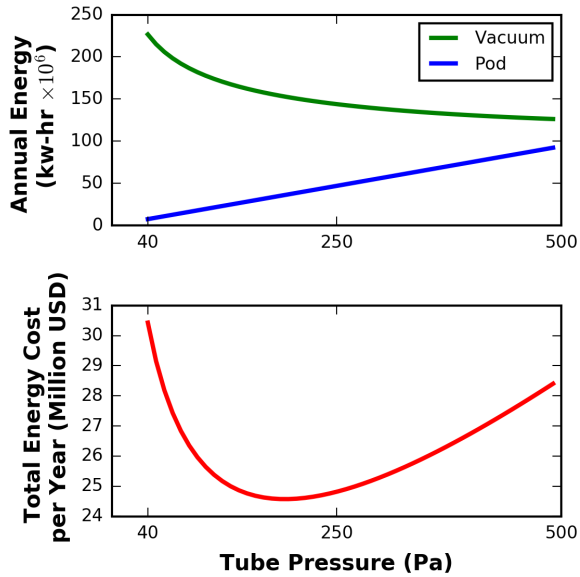

Figure 12: Energy Consumption and Cost vs. Tube Pressure

Figure 12 shows how the power and energy consumption change with tube pressure. As expected, high tube pressures require lower power for a given leakage rate while requiring a higher power output from the onboard compressor for a given compressor ratio. Thus total annual energy cost increases for very low pressures, due to the vacuum system managing the air leakage, and increases for very high pressures, due to increased power demand from the compressor. The second plot in fig. 12 shows that this relationship produces a pressure at which energy cost is minimal. In this case, the energy consumption is minimal at about 200 Pa for a leakage of 3 $\frac{kg}{s}$. Energy consumption increases fairly rapidly as pressure is increased beyond this minimum value. It is important to note that this exact value is dependent on the leakage rate, compressor pressure ratio, and whether or not regenerative braking is used to recover battery energy (no regenerative braking is assumed in this analysis). However, this relationship is crucial because it means that there exists a pressure that optimizes energy cost and that energy cost can increase rapidly if deviations from this optimum point exist. A higher fidelity model can be used to determine exactly what value of pressure optimizes energy consumption for a given configuration. A more detailed examination of the effects that leakage has on optimum pressure will be conducted next.

C. Leakage Rate

A major goal of this model is to study the effect that leakage has on optimal tunnel configuration. The Hyperloop infrastructure will be designed and manufactured with the goal of making the tube air tight; however, a perfectly air tight tube is not possible. Slight leakage flow rates are to be expected due to diffusion, desorption, permeation, leaks through micro cracks, and leaks in mechanical components. Furthermore, air will likely need to be introduced into the system to allow passengers to board. The leakage rate due to diffusion and permeation is proportional to the tube surface area while the air introduced into the system during passenger boarding is proportional to the frequency at which pods leave the station. While the exact leakage rate into the system is difficult to quantify, accounting for leakage provides valuable insight to performance of the system as a whole. The previous trade study showed that, for a given leakage rate, an operating pressure exists at which steady state energy consumption is minimal. The pressure at which this minimum occurs is a function of leakage rate. To evaluate the sensitivity of optimum pressure to leakage rate, the previous study will be repeated for a range of leakage rates. In each study, the pressure at which minimum energy consumption occurs will be determined using the ScipyOptimizer. The minimum value of total energy cost and the corresponding tube pressure will be recorded and plotted to evaluate the effects that leakage rate has on the system design variables.

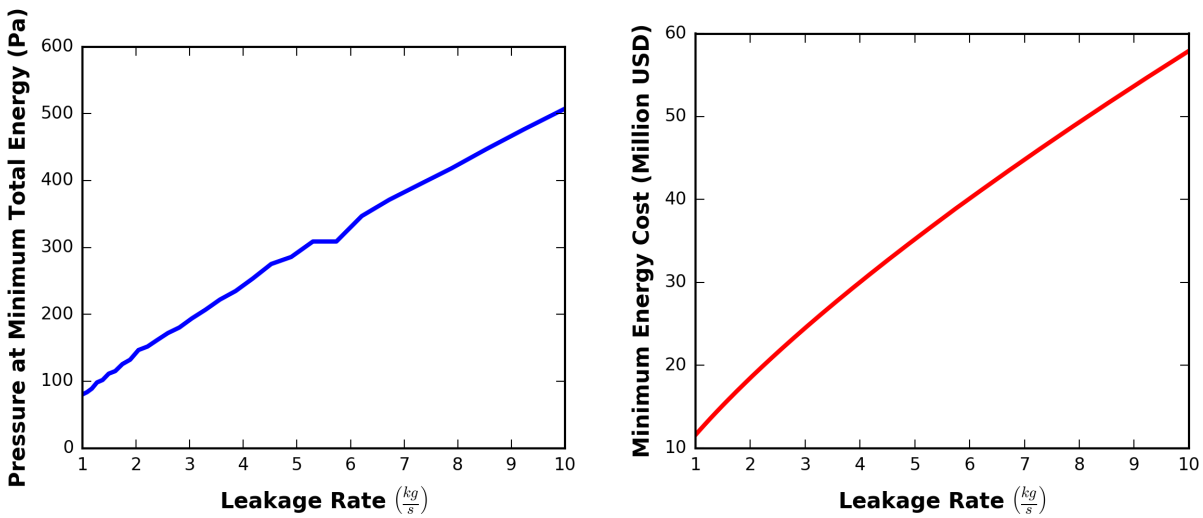

(a) Pressure at Minimum Energy vs. Leakage Rate (b) Minimized Energy Cost vs. Leakage Rate
Figure 13: Optimal pressures and resulting cost for a sweep of leakage rates

Figure 13 shows the pressure at minimum energy consumption and cost vs. the leakage rate of the tube. The tube pressure that optimizes cost increases as the leakage rate increases. This trend is reasonable because the increasing leakage rate increases the power required for the vacuum pumps to maintain the tube pressure, which is offset by increasing the pressure that the vacuum is required to maintain. This relationship is critical because it reveals a coupling between tunnel leakage and energy consumption that system designers must consider. As fig. 13 reveals, changes in the leakage rate can have a significant effect on energy consumption and energy cost. In fact, the cost penalty becomes even more substantial when operating at a suboptimal pressure. If the designer wants to optimize the system by minimizing the energy consumption, then more accurate modeling or empirical studies will be necessary to determine operating pressure. Furthermore, the assumption made that the leakage rate is constant is likely not indicative of a real system. Leakage, and therefore the optimal tunnel pressure, is also presumably a function of passenger pod frequency. System designers would need to account for variable tube pressure when sizing the battery, compressor motor, and tube diameter in order to give the operator flexibility to change the tube pressure with pod frequency. This would allow the Hyperloop system to adapt to changing operating conditions to more closely track optimal design configurations in real time. Further research with higher fidelity modeling is necessary to further characterize the benefits of variable tunnel pressure.

D. Capacity Trades

The original Hyperloop proposal suggested that the pod would likely be able to carry about 28 passengers.[2] To meet the market demand, the frequency at which pods depart could be increased or decreased as necessary. A high pod frequency could be problematic as it would require a large number of pods to be maintained at the end points and may not provide enough time for passengers to board comfortably. Thus, it is of particular interest to examine how the performance of the system is affected over a range of pod capacities. Increasing the capacity would allow the operator to have fewer pods taking off at a lower frequency to meet the market demanded passenger throughput. The overall benefits of changes in pod capacity can be more accurately determined by analyzing the sensitivity of energy consumption and operating cost to pod capacity. In this analysis, the number of passengers per pod is varied from 10 to 100. At each quantity, the estimated recurring energy cost and cost per capita are recorded.

Table 1 shows the relationship between yearly energy consumption and the number of passengers per pod produced by the system model. It is shown that, for the given operating condition, an order of magnitude increase in pod capacity only results in a 15% increase in yearly energy consumption. This, in conjunction with the previously discussed structural analysis, indicates that the cost associated with changing pod capacity is small. This relationship is significant because it means that the Hyperloop operator can specifically set the pod capacity to whatever value is necessary to meet a particular market demand, without costly changes

Passengers Per Pod	10	20	30	40	50	60	70	80	90	100
Energy Cost ($M)	28.2	28.6	29.0	29.5	29.9	30.3	30.7	31.1	31.6	32.0
Total $/Passenger	226	113	76	57	45	38	33	29	25	23

Table 1: Energy cost for various pod capacities

in performance or design. Furthermore, this makes it possible for future researchers to consider making Hyperloop pods modular. It is possible that, instead of having one large pod carrying a fixed number of passengers, the operator could have multiple pods that carry a small number of passengers. Each of these pods would link together until the capacity of each individual flight matched demand. This would allow the Hyperloop to handle high densities of passengers during peak travel times without having to increase pod frequency to prohibitive levels. Then, during lighter travel times, the operator could link fewer pods together to reduce the gross weight of each flight in order to reduce unnecessary energy consumption. The cost per passenger also rapidly declines, before tapering off at capacities not suited for the tube pressure chosen for this particular parameter sweep.

V. Conclusion

Using various Python libraries and CFD packages, an open-source model of the Hyperloop was created to evaluate system and subsystem level engineering and cost trade studies with the overall goal of better characterizing the concept. The key subsystem models included structural analyses of the travel tube, RANS CFD based drag model for the passenger pod, electromagnetic analysis of the levitation system, an empirical battery model, thermodynamic analysis of the vacuum pumping system, and a numerical integration based mission analysis. The trade studies provides several key conclusions about the sensitivity of Hyperloop to key design parameters. A subsystem analysis of the structural requirements for the tube showed that underwater routes could have a significantly lower materials cost due to a more favorable loading conditions generated by buoyancy.

A full model system study was performed to analyze the net energy usage of maintaining the tube operating pressure as a function of the leakage rate of air into the tube. The results show that the energy usage from this system is of the same order of magnitude as the energy required to propel the passenger pod. Furthermore, the two systems have opposite sensitivities with respect to tube pressure. As the tube pressure is lowered, the energy needed to propel the pod drops, but the energy required to maintain the vacuum goes up. The results show that there is an optimal tube operating pressure that is heavily dependent on the leakage rate. The higher the leakage rate is, the higher the optimal tube operating pressure becomes.

This work also extends previous research that shows traveling at speeds above Mach 0.8 is likely not practical. The tube size invariably becomes too large, given the coupling between tube size and pod travel speed. We refine that analysis to include the effects of boundary layer growth along the passenger pod. The data shows that boundary layer growth amplifies the coupling between tube size and travel speed and hence is an important consideration in Hyperloop design. As a result, further research on the modeling and implementation of active flow control is recommended due to its potential to significantly reduce required tube size.

Finally, net energy usage is found to be relatively insensitive to pod length. Therefore, the system would scale favorably to much higher passenger capacities than originally proposed. This also gives the operator freedom to vary capacity by lengthening or shortening pods, meaning travel capacity can be optimized to meet market demand without prohibitive costs to the operator.

Although the models presented in this paper are not of high fidelity, the trends and trade studies identified provide valuable insight into the engineering behind the Hyperloop concept and how these physical relationships can inform future design efforts. The open source, modular nature of this system model will allow future researchers to modify, adapt, and improve the model to include more specific subsystems and higher fidelity modeling as needed. The modeling platform is intended to serve as a publicly accessible baseline that is easy to expand and delve deeper into this unique multidisciplinary system.

Appendix

A. Links to Source Code and Documentation

Source Code: `https://github.com/NASA-MARTI/MagnePlane`
Documentation: `http://magneplane.readthedocs.io/en/latest/`
Wiki: `https://github.com/NASA-MARTI/MagnePlane/wiki`

B. Model Overview (Continued)

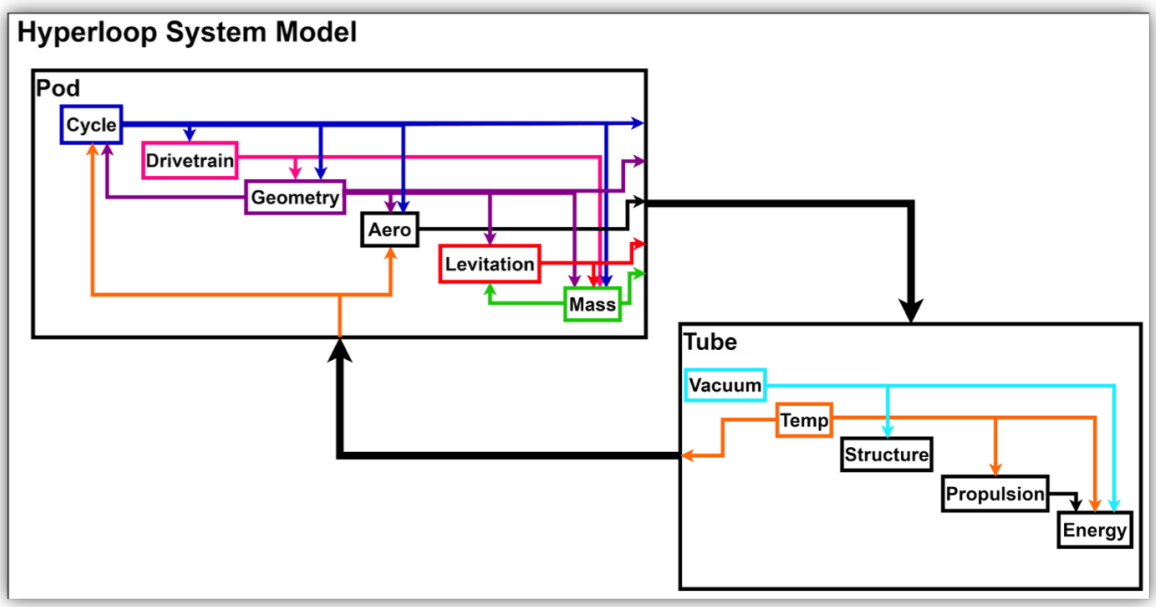

Figure 14: Connection diagram for entire system model

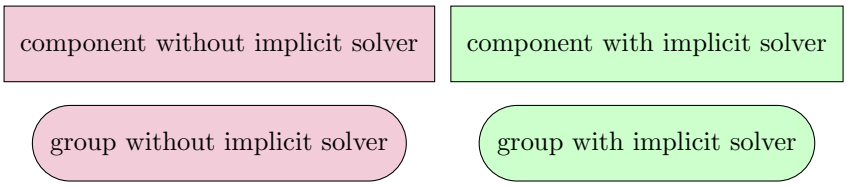

Figure 15: XDSM Diagram Key

Acknowledgements

The authors would like to thank the NASA Aeronautics Research Mission Directorate leadership, as well as Director of Strategy Therese Griebel and Glenn Academy Director David Kankam for funding the Multidisciplinary Aeronautics Research Team Initiative (MARTI) program. Additional thanks to Jerry Welch, Tom Gregory, Isaiah Blankson, Kenneth T Moore, Keith Marsteller, and Scott Jones for their mentorship and guidance.

References

[1]Jeffrey Chin, Justin Gray, Scott Jones, and Jeffrey Berton. Open-source conceptual sizing model of the hyperloop passenger pod. *AIAA Science and Technoloy Exposition*, 2014.

[2]Elon Musk. Hyperloop alpha. Website, August 2013.

[3]Andreas Schafer and David Victor. The future of mobility of the world population. *Transportation Research*, Part A 34:171–205, 2000.

[4]Hojong Baik, Antonio Trani, Nicolas Hinze, Howard Swingle, Senanu Ashiabor, and Anand Seshadri. Forecasting model for air taxi, commercial airline, and automobile demand in the united states. *Transportation Research Record: Journal of the Transportation Research Board*, (2052):9–20, 2008.

[5]Robert M. Salter. The very high speed transit system. *RAND Corporation P-4874*, 1972.

[6]Catherine Taylor, David Hyde, and Lawrence Barr. Hyperloop commericial feasability analysis. Technical report, U.S. Department of Transportation, 2016.

[7]Paul Friend. Magnetic levitation train technology 1. *progress report, Bradley university*, 2004.

[8]US EIA. Annual energy outlook 2013. *US Energy Information Administration, Washington, DC*, pages 60–62, 2013.

[9]R. T. Biedron, J. M. Derlaga, P. A. Gnoffo, D. P. Hammond, W. T.Jones, B.Kleb, E. M. Lee-Rausch, E. J. Nielsen, M. A. Park, C.L. Rumsey, J. L. Thomas, and W. A. Wood. FUN3D manual: 12.4. *NASA TM-2014-218179*, 2014.

[10]P. L. Roe. Approximate riemann solvers, parameter vectors, and difference schemes. *Journal of Computational Physics*, 43(2):357–372, October 1981.

[11]P. R. Spalart and S. R. Allmaras. A one-equation turbulence model for aerodynamic flows. *La Techerche Aerospatiale*, 1:5–21, 1994.

[12]D. Marcum. Generation of unstructured grids for viscous flow applications. *AIAA Paper No. 95-0212*, 1995.

[13]Justin Gray, Jeffrey Chin, Tristan Hearn, Eric Hendricks, Thomas Lavelle, and Joaquim R. R. A. Martins. Thermodynamics of gas turbine cycles with analytic derivatives in openmdao. *AIAA SciTech*, Jan 2016.

[14]Collins Gladin, Ali. Conceptual modeling of electric and hybrid-electric propulsion for UAS applications. Sep 2015.

[15]Marty K Bradley and Christopher K Droney. Subsonic ultra green aircraft research. 2011.

[16]Jacek F Gieras, Zbigniew J Piech, and Bronislaw Tomczuk. *Linear synchronous motors: transportation and automation systems*. CRC press, 2016.

[17]Justin Gray, Kenneth T. Moore, Tristan A. Hearn, and Bret A. Naylor. Standard platform for benchmarking multidisciplinary design analysis and optimization architectures. *AIAA Journal*, 51(10):2380–2394, Oct 2013.

[18]Eric Jones, Travis Oliphant, Pearu Peterson, et al. Scipy: Open source scientific tools for Python, 2001. [Online; accessed 2016-09-26].

[19]JP Peterson. Buckling of thin-walled circular cylinders. (NASA Technical Report Server, SP-8005), 1968.

[20]Robert W. Fox, Philip J. Pritchard, Alan T. McDonald, and Robert W. Fox. *Fox and McDonald's introduction to fluid mechanics*. John Wiley Sons, Inc., 2011.